Article

# Chemoenzymatic Labeling of Extracellular Vesicles for Visualizing Their Cellular Internalization in Real Time

Ying Jiang, Lei Wang, Pengjuan Zhang, Xuehui Liu, Huixia Di, Jie Yang, Shu-Lin Liu, Dai-Wen Pang, and Dingbin Liu

*Anal. Chem.*, **Just Accepted Manuscript** • DOI: 10.1021/acs.analchem.9b04608 • Publication Date (Web): 26 Dec 2019

# Chemoenzymatic Labeling of Extracellular Vesicles for Visualizing Their Cellular Internalization in Real Time

Ying Jiang, Lei Wang, Pengjuan Zhang, Xuehui Liu, Huixia Di, Jie Yang, Shu-Lin Liu, Dai-Wen Pang, and Dingbin Liu*

College of Chemistry, Research Center for Analytical Sciences, Institute of Polymer Chemistry, State Key Laboratory of Medicinal Chemical Biology, and Tianjin Key Laboratory of Molecular Recognition and Biosensing, Nankai University, Tianjin 300071 (China)

*Supporting Information Placeholder*

**ABSTRACT:** Extracellular vesicles (EVs) are intercellular communicators that are heavily implicated in diverse pathological processes. However, it is poorly understood how EVs interact with recipient cells due to the lack of appropriate tracking techniques. Here, we report a robust chemoenzymatic labeling technique for visualizing the internalization process of EVs into target cells in real time. This method uses phospholipase D (PLD) to catalyze the in-situ exchange of choline by alkyne in the native EV phosphatidylcholine. Subsequent alkyne−azide click chemistry allows conjugation of Cy5 dyes for visualizing EVs internalization by confocal fluorescence microscopy. The fluorescent labeling of EVs was accomplished in an efficient and biocompatible way, without affecting both the morphology and biological activity of EVs. We applied this chemoenzymatic labeling strategy to monitor the cellular uptake of cancer cell-derived EVs in real time and to further reveal multiple internalization mechanisms. This robust, biocompatible labeling strategy provides an essential tool for EV-related studies ranging from chemical biology to drug delivery.

## INTRODUCTION

Extracellular vesicles (EVs), ranging from 50 to 1000 nm in size, are membrane-like nanoparticles that contain complex molecules derived from parental cells, including proteins, nucleic acids, lipids, and carbohydrates, etc.[1,2] EVs act as natural carriers that transport molecular information from parental cells to recipient cells.[3-5] Thus, they play significant roles in regulating diverse pathological and physiological functions of recipient cells such as cancer metastasis, inflammation, and tissue regeneration.[6-9] Besides, EVs can serve as drug delivery platforms that show distinct properties in overcoming the blood-brain barrier (BBB), along with high stability and biocompatibility.[1,9] Therefore, elucidating the pathophysiological roles of EVs in biological systems is of great significance to both basic and clinical studies.[10-15] However, the processes by which the EVs are taken up by recipient cells have not been well understood, due to the lack of appropriate tracking techniques. The development of simple but powerful labeling methods is the key to reveal the mechanisms of EVs uptake by cells.

Because of their small size and complex biological compositions, EVs are difficult to be labeled. The existing labeling strategies are mainly based on the modification of EV proteins or lipids.[16] The protein labeling methods depend on either genetic engineering of an overexpressed fluorescent protein (such as GFP) inside cells or chemical conjugation of the membrane proteins with fluorescent dyes.[17-19] These methods are often tedious or/and could impair the biological activity of EVs during uptake. Lipid modification strategies have recently attracted immense interest for EV labeling owing to their ease of functionalization and excellent biocompatibility. The most commonly used lipid labeling method for EVs relies on incorporating the hydrophobic layer of EV membrane with specific dyes, such as lipophilic dyes (PKH26, PKH67)[20,21] or carbocyanine dyes (DiI, DiO)[22,23]. These dyes are assembled into the EV membranes through a non-covalent way, which is unstable in physiological environments and thus causes dyes leaching from the EV membrane. Moreover, these dyes could form aggregates or micelle structures in aqueous solution, providing misleading information in the EV uptake experiments.[24-26] These issues could be addressed if the dyes are labeled covalently on the EV phospholipids. However, the phospholipids show low reaction activity, making them difficult to be modified chemically. To date, the covalent phospholipid labeling strategy often refers to metabolic labeling,[27] which requires tedious, time-consuming cell culture and multi-step experimental operations. Therefore, it is highly desirable to develop a simple covalent phospholipid modification strategy for EV labeling.

In this study, we report a chemoenzymatic-assisted covalent modification strategy which allows the direct labeling of EV phosphatidylcholine via a simple two-step process (**Figure 1**). The phospholipid headgroups (cholines) in the EV membranes are exchanged with alkynes by the catalysis of phospholipase D (PLD) enzymes, followed by click chemistry with an azido fluorophore to enable fluorescent labeling of the EVs. Due to the high performance of PLD catalysis and the high efficiency of click chemistry, this direct labeling strategy towards EVs is simple but powerful, without resorting to time-consuming procedures such as cell culture. We demonstrated the application of this strategy into monitoring the biological interactions between cancer cell-derived EVs and macrophage

cell line (RAW264.7 cell), and revealed their internalization mechanisms using different inhibitors.

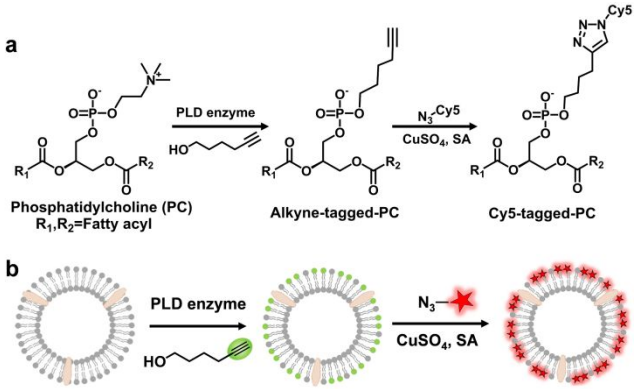


**Figure 1.** Illustration of the chemoenzymatic labeling strategy. (a) Molecular description of the two-step labeling approach. SA, sodium ascorbate. (b) Labeling extracellular vesicles using the transphosphatidylation reaction mediated by PLD enzyme and alkyne−azide click chemistry.

## EXPERIMENTAL SECTION

**Materials and reagents.** 1,2-dioleoyl-sn-glycero-3-phosphocholine (DOPC) was purchased from Ruixi Biological Technology Co. Ltd (Xi'an, China). Az-Cy5 (Azide-Cy5), NHS-Cy5 (N-Hydroxysuccinimide Cy5) and Arachis hypogaea PLD were purchased from Sigma-Aldrich (St. Louis, USA). DiI, EIPA, Wortmannin and Dynasore were purchased from MedChemExpress (NJ, USA). Chlorpromazine and Cytochalasin D were purchased from Cayman Chemical (Ann Arbor, Michigan). MCF-7 and RAW264.7 cell lines were obtained from Shanghai Institute of life sciences, Chinese Academy of Sciences (Shanghai, China). Dulbecco's modified Eagle medium (DMEM), Fetal bovine serum (FBS), 0.05% trypsin-EDTA and antibiotics (penicillin-streptomycin) were purchased from Gibco (Grand Island, NY). Dulbecco's phosphate-buffered saline (D-PBS) was purchased from Genview (TX, USA).

**PLD-catalytic transphosphatidylation reaction toward DOPC.** 10 μL of 8 mg/mL DOPC in chloroform was placed in a 2 mL Eppendorf tube. The chloroform was blown dry by a stream of argon. The tube was then added with 1.5 μL of 50 mM SDS (Sigma-Aldrich), 3 μL of 1 M sodium acetate (pH 5.6) (Meryer, Shanghai) and 25 μL of 90 mM 5-hexyn-1-ol (Aladdin, Shanghai) in water. Subsequently, 3 μL of 500 mM $CaCl_2$ (Meryer, Shanghai) and 2 μL of deionized water were added under vortex, followed by adding 2 μL of Arachis hypogaea PLD (2 U/μL). The resulting mixture was incubated at 30 °C for 90 min. Afterward, the solution was added with 70 μL of PBS, 250 μL of methanol, 250 μL of chloroform, and 125 μL of 20 mM HAc (Hengan Chemical, Jiangsu). This solution was vortexed for 1 min and then centrifuged for 2 min at 16,000 g. The organic layer was collected while the aqueous layer was transferred to a new tube and then mixed with 250 μL of chloroform. The mixture was vortexed and centrifuged once again to yield a solution consisting of organic and aqueous layers. Finally, the two organic solutions were combined and dried under a stream of $N_2$. The products were re-suspended in 100 μL methanol and measured by LC-MS, which was performed on a Waters ACQUITY UPLC SYNAPT G2-Si QTOF system with BEH HILIC columns.

**Cell culture.** Mouse mononuclear macrophage leukemia cell line RAW264.7 and human breast cancer cell line MCF-7 were cultured in Dulbecco's modified Eagle's medium (DMEM, Gibco) supplemented with 10% EV-depleted FBS, 1% penicillin/streptomycin (Gibco). Cell cultures were incubated in a 5% $CO_2$ incubator at 37 °C.

**Chemoenzymatic labeling of the cells.** The MCF-7 cells with a density of $1\times10^5$ were seeded in 48-well plate (Nest, China) with cell slides and incubated in 5% $CO_2$ incubator at 37 °C overnight. Then, 2 μL of 90 mM 5-hexyn-1-ol and 2 μL of Arachis hypogaea PLD (2 U/μL) was added to each well. The reaction was placed in a 30 rpm shaker for 30 °C. After 3 h, the media were removed and the wells were washed with D-PBS for three times. Subsequently, 84 μL of D-PBS, 5 μL of 20 mM $CuSO_4$ (Heowns, Tianjin), 10 μL of 500 mM sodium ascorbate (Aladdin, Shanghai), and 1 μL of 1 mM $N_3$-Cy5 were added to each well. After Incubation at 40 °C for 2 h, the media were discarded and the wells were washed with D-PBS for three times. Finally, the cells were fixed by 4% paraformaldehyde and the nuclei were stained with 10 μM DAPI (Solarbio, Beijing) for 3 min. The cells were observed by fluorescence microscope (Leica) with 40× objective lens.

**Isolation, purification, and characterizations of EVs.** After culturing for 48 h, the media for MCF-7 cells were first centrifuged at 2000 g for 10 min to remove dead cells and cell debris. Subsequently, the supernatants were collected and further centrifuged at 10,000 g for 30 min to yield purified EVs. The EVs were re-suspended in D-PBS, where their protein concentration was measured by BCA kit (Beyotime Biotechnology). The morphology of EVs was characterized by transmission electron microscopy (Talos F200C, FEI). The hydrodynamic sizes and zeta potential of EVs were analyzed by the nanoparticle Analyzer (Zetasizer Nano ZS, Malvern Instruments) and nanoparticle tracking analyser ZetaView PMX 110 (Particle Metrix, Meerbusch, Germany).

**Western Blot Assays.** EVs and Cy5-EVs were lysed by ice-cold RIPA buffer (Beyotime Biotechnology) with a protease inhibitor (PMSF, 1mM, Beyotime Biotechnology) for 30 min. Then the lysates were centrifuged at 14,000 g for 20 min at 4 °C and supernatant were achieved for the BCA assay and used for western blot assays. Samples were separated by SDS-PAGE and then transferred onto a 0.45 μm nitrocellulose membrane (Beyotime Biotechnology). Subsequently, the membrane was blocked with 5% skim milk (in TBST, 20 mM Tris-HCl, 150 mM NaCl, and 0.1% Tween-20) at 37 °C for 1 h. Then the membranes were incubated with primary antibody for western blot analysis: Anti-Alix (1:1,000, abcam; ab117600), Anti-Annexin A1 (1: 1,000, abcam; ab135256), Anti-Tsg101 (1:1000, abcam, ab83), Anti-CD63 (1:1000, proteintech, 25682). Anti-mouse IgG, HRP-linked antibody (1: 3,000, abcam; ab205719) and anti-rabbit IgG, HRP-linked anti-body (1: 3,000, abcam; ab6721) were used as secondary anti-bodies. The membranes for primary antibodies incubation were 4 °C overnight and washed three times with TBST for 5 min each and then incubated with secondary antibodies at 37 °C for 2 h. Then the membranes were washed three times with TBST for 10 min each. Finally, the membranes were incubated with BeyoECL Plus (Beyotime Biotechnology) and imaged with Azure c600 (Azure Biosystems, USA).

**Characterizations of alkyne-modified EVs.** 80 μg of EVs isolated from MCF-7 cell culture supernatants were diluted in 200 μL phosphate buffer (pH 5.6). Then, 2 μL of 5-hexyn-1-ol (90 mM) and 2 μL of Arachis hypogaea PLD (2 U/μL) were added to the EVs solution. The reaction was placed in a thermostatic metal bath at 30 °C for 3 h. After that, the unreacted small molecules were removed under 10,000 g centrifugation for three times. The alkyne-labeled EVs were re-suspended in D-PBS for further use.

***Characterization of EVs with surface-enhanced Raman spectroscopy (SERS).*** To measure the chemical groups on EV membranes with SERS, a rough gold substrate should be fabricated as Raman enhancer. Briefly, a glass slide was immersed in 3 mM $HAuCl_4$ followed by adding ammonium hydroxide at 20 μL ammonium hydroxide per mL of $HAuCl_4$ solution with rapid shaking for 1 minute. The slide was washed twice with deionized water to remove unbound gold ions and incubated with 1 mM $NaBH_4$ solution to generate gold seeds. After further washing twice with water, the gold seed-bearing slide was immersed in a solution of $HAuCl_4$ and hydroxylamine at a 1:1 ratio and shaken for 5 min, followed by a 10 min incubation to yield a rough gold nanoparticle-immobilized SERS substrate. After washing the substrate with DI water twice and drying, the concentrated EVs were dropped to the SERS substrate and dried under 37 °C incubator for 10 min. Then, the Raman spectra were recorded by a confocal Raman spectrometer with 633 nm excitation light source (0.5 mW), 50× objective lens, and an exposure time of 10 s.

***Fluorescent imaging of EVs.*** The EVs were re-suspended by 200 μL of D-PBS. Then, 2 μL of 1 mM $N_3$-Cy5, 10 μL of 20 mM $CuSO_4$, and 20 μL of 500 mM sodium ascorbate were added to the EVs solution. After incubating in 40 °C metal bath for 2 h, the reaction was centrifuged under 10,000 g for 30 min. The EVs were co-stained with 5 μM of DiI dyes for 5 min and then washed with PBS for three times. The samples were dropped on a glass slide, where the fluorescent EVs were observed by A1+ confocal fluorescence microscope (Nikon, Japan) with 100× objective lens. Moreover, the Cy5-labeled EVs were diluted in 200 μL D-PBS and measured by F-4600 fluorescence spectrophotometer (Hitachi, Tokyo).

**The purity testing of Cy5-modified EVs using the sucrose density gradient centrifugation assay.** Different density of sucrose solution (30%, 40%, 50%, 60%, 200 μL) were paved into 2 mL Eppendorf tube for four layers carefully and the double-stained EVs (20 μL) were added in the upper layer. Then, the sample was centrifuged by 10,000 g for 30 min. After centrifugation, the liquid was divided for four fraction by pipette (200 μL/fraction, from top to bottom). Each fraction was imaged by Azure c600 and analyzed by F-4600 fluorescence spectrophotometer.

**Wound healing assay.** $3\times10^5$ MCF-7 cells were seeded on 24-well plate (Nest, China) and incubated in 5% $CO_2$ incubator at 37 °C overnight. When confluence reached 100%, the cell monolayers were scratched using a pipette tip. Then, the cells continued to grow in replaced media in the presence of EVs under different conditions. For each group, about 10 μL of EVs (0.4 mg/mL) was added. Afterward, the plate was put back to 5% $CO_2$ incubator. The healing situation of each group was observed at 0 h and 18 h under a fluorescence microscope (Leica) with 10× lens. ImageJ was used to calculate the wound width of the scratches.

**Evaluation of the chemical stability of EV labeling in sera.** EV labeled with Azide-Cy5 or DiI dye were incubated in D-PBS containing 20% fetal bovine serum (FBS)[28] at 37 °C for 1 h or 12 h. Subsequently, samples were subjected to centrifuge by 10,000 g, which allows separation of the dye-labeled EVs and corresponding supernatants. The fluorescence of dye-labeled EVs and supernatants was obtained with F-4600 fluorescence spectrophotometer.

**SPT (Single-particle tracking) in living cells.** RAW264.7 cells were seeded onto a 35 mm glass-based dish overnight prior to observation and incubated with Cy5-EVs (20 μL, 0.4 mg/mL) at 4 °C for 10 min for attachment. Excess EVs were removed by washing with D-PBS. SPT was performed on a Leica DMi8 microscope with an Andor Dragonfly confocal unit. All images were acquired with a Leica 100× oil immersion objective with a numerical aperture of 1.4 and Andor iQ software. We selected a 640 nm laser with a BP 700/50 nm filter for Cy5. The movements of labeled EVs were tracked and analyzed using Image Pro Plus (IPP). The trajectories of labeled EVs were generated by tracking the representative single EV. Mean square displacement (MSD) was calculated using a home compiled program based on Matlab (MathWorks).

**Long-term monitoring of Cy5-EVs internalization by RAW264.7 cells and MCF-7 cells.**

***Confocal fluorescence microscope.*** RAW264.7 cells and MCF-7 cells with a density of $2\times10^5$ were seeded into confocal dishes (φ20 mm) (Nest, China) and incubated in a cell incubator overnight. The internalization process was carried out in an incubator with 5% $CO_2$ at 37 °C. 20 μL of Cy5-labeled EVs (0.4 mg/mL) was added to adhered RAW264.7 cells and MCF-7 cells for monitoring at 0, 20, 40 min, and 1, 2, 4, 8, and 12 h, respectively. Before imaging, the cells were fixed with 4% paraformaldehyde (PFA) and co-stained by incubation with 500 μL of 10 μg/ml Hoechst 33342 (Solarbio, Beijing) for 4 min. For 3D imaging, 5 μM of DiI was first used to stain the cell membranes for 6 min after the cell culture was removed, then the cells were fixed and stained by Hoechst 33342. The fluorescent images were acquired by A1+ confocal fluorescence microscope (Nikon, Japan) with 60× objective lens.

***Flow Cytometry.*** The same density of RAW264.7 cells and MCF-7 cells as above was seeded in 35 mm culture dishes (Corning, USA) and incubated at 37 °C overnight. Then, 20 μL of Cy5-EVs (0.4 mg/mL) was added to each dish and incubated for 0, 20, 40 min, and 1, 2, 4, 8, 12 h, respectively. After the incubation, the media were removed and the cells were digested, finally fixed with 4% PFA and tested under flow cytometry (BD LSR Fortessa) with excitation at a wavelength of 640 nm. 10,000 cells were used for each sample. Flowjo was used for data presentation.

**Revealing EV uptake mechanisms with various endocytosis inhibitors.** RAW264.7 cells were first seeded into 35 mm culture dishes and then cultured overnight. Then, different doses of inhibitors including cytochalasin D, EIPA, wortmannin, chlorpromazine, and MβCD were added to the cells respectively and incubated for 30 min. Subsequently, 20 μL of Cy5-labeled EVs (0.4 mg/mL) was added to the cells and incubated for 4 h. Then, the cell media were removed and the cells were washed by D-PBS three times. Afterward, the cells were digested, fixed with 4% PFA overnight and measured by

flow cytometry (BD LSR Fortessa) with excitation at a wavelength of 640 nm. 10,000 cells were used throughout all the samples.

## RESULTS AND DISCUSSION

Our study was inspired by the fact that PLD enzymes are able to hydrolyze phosphatidylcholine into phosphatidic acid and choline under physiological conditions.[29] In the presence of primary alcohols, PLD enzymes can also catalyze the transphosphatidylation reaction of phosphatidylcholine to produce unnatural phosphatidyl alcohols. With this principle, we would like to conduct the transphosphatidylation reaction with alkyne-bearing alcohols (namely alkynol), by which the EV membranes could be introduced with alkynes for click labeling.[30-32] To evaluate the feasibility of this hypothesis, 1,2-dioleoyl-sn-glycero-3-phosphocholine (DOPC) was mixed with excessive 5-hexyn-1-ol (a typical alkynol) under the catalysis of a commercially available PLD. DOPC is classical synthetic phosphatidylcholine whose molecular structure is close to the natural phosphatidylcholine.

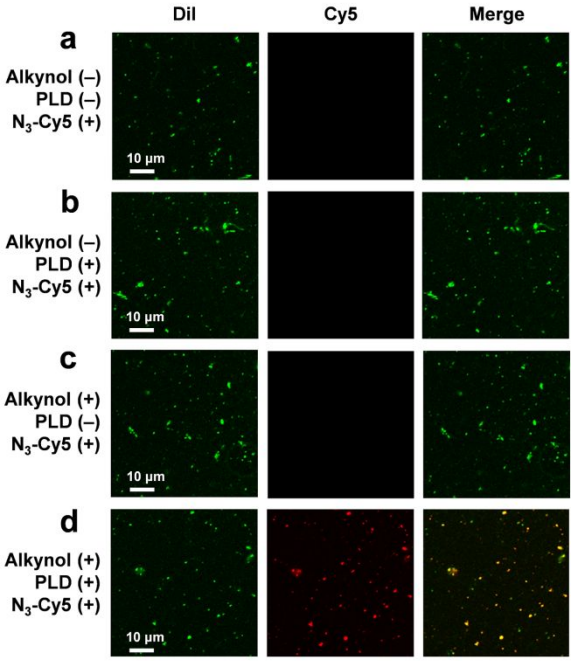


**Figure 2.** Fluorescence contrast images of MCF-7 cell-secreted EVs after fluorescent labeling under different conditions. (a) The intact EVs (200 μL, 0.4 mg/mL) were added with $N_3$-Cy5 dyes (2 μL, 1 mM) directly in the absence of alkynol and PLD. The same amount of intact EVs were first added with either PLD enzyme (2 μL, 2 U/μL) (b) or 5-hexyn-1-ol (2 μL, 90 mM) (c), and then added with $N_3$-Cy5 dyes. (d) The intact EVs were first incubated with both PLD enzyme and 5-hexyn-1-ol, and then incubated with $N_3$-Cy5 dyes. The concentrations for each kind of reagents used in different conditions were fixed to be the same. EVs were co-stained with DiI dyes (1 μL, 1 mM) as a contrast. The images were captured by Nikon A1+ confocal fluorescence microscope with 100× lens.

The results show that the choline in DOPC was exchanged by alkyne quickly, and the reaction was completed in 90 min. The typical structures of DOPC and its alkyne-bearing product are found in Supplementary **Figure S1**. The alkyne-bearing DOPC products were seperated by HPLC and identified by mass spectrometry under anion mode ([M–H] $^-$). The results were compared to that of DOPC itself (Supplementary **Figures S2,3**). As observed from the mass spectrum, three molecular weights are found at 820.56, 830.59, and 844.61 m/z, which are attributed to DOPC (EM 785.59) coupled by the negatively-charged ions [$Cl^-$], [$HCOO^-$], and [$CH3COO^-$], respectively. In contrast, the molecular weight for the alkyne-bearing DOPC products was found at 779.55 m/z (calculated 779.56). The decrease of molecular weights in the mass spectra proved that the enzyme-assisted modification of DOPC can be achieved successfully in tubes.

Next, we examined the labeling strategy towards the natural phosphatidylcholine in cell membranes. Excessive 5-hexyne-1-ol and PLD were first incubated with MCF-7 cells adhered on a cell-culture plate. After 3 h, the free 5-hexyne-1-ol and PLD were removed, and the resulting alkyne-appended cells were then conjugated with azido-bearing Cy5 ($N_3$-Cy5) dyes via click chemistry. Only the addition of 5-hexyne-1-ol, PLD, and $N_3$-Cy5 enabled fluorescent labeling of the cell membranes (Supplementary **Figure S4**); while in the absence of either 5-hexyne-1-ol or PLD, $N_3$-Cy5 was unable to light up the cell membranes, indicating excellent specificity of the reactions.

Encouraged by the above experimental results of feasibility testing, we subsequently applied the modification strategy into EVs labeling. Note that we employed this chemoenzymatic strategy to label larger sizes of EVs, because they are easy to be enriched under low-speed centrifugation and to be visualized by confocal fluorescent microscope. To modify the EV membranes, the EVs derived from MCF-7 cells were mixed with the solution of 5-hexyne-1-ol and PLD directly. After purification with centrifugation, the resulting alkyne-labeled EVs were characterized by Raman spectrometry. A single band was clearly observed at around 2100 $cm^{-1}$ (Supplementary **Figure S5**), which is ascribed to the exogenous alkyne group,[33] demonstrating the successful labeling of alkynes into the EV membranes. Further, $N_3$-Cy5 dyes were conjugated to the alkyne-tagged EVs membrane by click chemistry. Moreover, we also wondered if the free fluorescent dyes had been washed away thoroughly. We first stained the EVs with both DiI and Cy5, followed by washing with PBS for three times. The resulted mixtures were seperated by the sucrose density gradient centrifugation assay. After centriguation, we can observe that the fluorescence singal only appeared in fraction 3 (Supplementary **Figures S6** and **S7**). The results prove that the free dyes had been washed off and the fluorescent signals were only derived from the labeled EVs. The fluorescent labeling of EVs was confirmed by testing the fluorescent intensity of the EV particles in PBS, as indicated by a strong fluorescence emission of Cy5 at 670 nm (Supplementary **Figure S8**). Additionally, the Cy5 fluorescence of EVs can also be recorded by a confocal fluorescent microscope (**Figure 2**). The Cy5 signals are fully overlapped with that of DiI dyes that were non-covalently incorporated into the EV membranes as a contrast. These results validate that the EV membranes can be fluorescently labeled via the covalent chemoenzymatic strategy. With the aid of flow cytometry analysis, we found that the labeling effeciency of Cy5-EVs achieved 62.4% (Supplementary **Figure S9**).

Additionally, an ideal labeling approach should possess high biocompatibility. We thus wanted to know whether the chemoenzymatic labeling strategy could impact both the morphology and biological activity of the EVs. First, we employed transmission electron microscopy (TEM) to analyze

the morphology of EVs and Cy5-EVs (**Figure 3a,b**). The TEM images display that EVs retained representative saucer-shaped morphology, which means that the integrity of the vesicles was not damaged or changed during the modification process. Similarly, NTA data and DLS data confirmed that the nanoscale hydrodynamic sizes of EVs have no significant changes before and after the chemoenzymatic labeling (**Figure 3c,d** and Supplementary **Figure S10**). Moreover, the zeta potentials of EVs and Cy5-EVs also had no obvious change ( Supplementary **Figure S11).** We further identified the characteristic proteins of the labeled EVs with western blot analysis and compared the results with the native EVs. After incubation with Alix, CD63, and Annexin A1 antibodies (a marker of microvesicles),[34] three characteristic bands appeared at 96 kDa, 26 kDa, and 39 kDa, respectively for all samples (Supplementary **Figure S12**), confirming that the labelling strategy has no obvious influence on the morphology and protein composition of EVs.

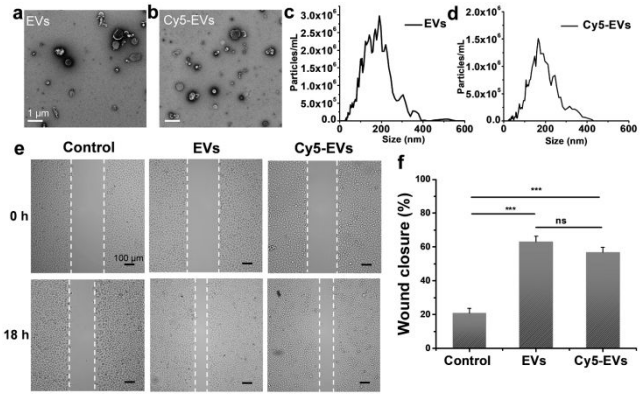


**Figure 3.** Morphological characterizations and biological activity testing for the native and labeled EVs secreted by MCF-7 cells. (a-b) TEM images of EVs and those chemoenzymatically labeled with Cy5 dyes. (c-d) Size distribution profile of EVs and Cy5-EVs measured by NTA. (e) Wound healing assays for the EVs and Cy5-EVs after incubation with MCF-7 cells for 18 h. The white dotted lines indicate the scratch edges. The Images were acquired under a microscope with a 10× objective lens. Scale bar: 100 μm. (f) Wound closure for the three scratches in the cell groups that was treated with EVs and Cy5-EVs for 18 h. The group without any EVs treatment was set as a control. Error bars indicate mean standard deviations of six images for each group (n = 6, ns = not significant or $p>0.05$; **, $p<0.01$; ***, $p<0.001$, two-tailed t-test).

A cell migration assay was employed to assess the influence of the labeling strategy on the biological activity of EVs. Considerable studies have discovered that EVs can transmit diverse molecular information (proteins, DNA, RNA, etc.) from the parental cells to the recipient cells, thus boosting cell migration between cell populations. Therefore, cell migration assays are broadly used to estimate the biological activity of EVs.[35,36] The scratched MCF-7 monolayers were incubated with 10 μL of native EVs (0.4 mg/mL) or the same amount of Cy5-labelled EVs. The cell scratch without the treatment of EVs was set as the control. The width of all initial scratches was defined to be 100%. After 18 h incubation, all the scratch width shrank as the growth of cells. Of note, the cell scratches reduced dramatically with the aid of EVs in comparison to the control (**Figure 3e**). However, there was no significant difference between the width of cell scratches that had been treated with native EVs and Cy5-labelled EVs. The average scratch healing rate for the native EV-treated group was 63%, while that for the labeled EV-treated group was 57% (**Figure 3f**). The two EV-treated groups exhibited an equal biological activity ($p>0.05$; two-tailed t-test) in promoting cell proliferation. By contrast, the untreated group showed an average scratch healing rate of 21%, much slower than that treated with both EVs. The cell migration assay verifies that the chemoenzymatic labeling strategy has a negligible impact on the biological activity of EVs.

The chemical stability of the chemoenzymatic labeling strategy was further investigated and compared to conventional phospholipid-based approaches. Currently, the most common labeling reagents for cell/EV membrane refer to commercially-available membrane dyes such as DiI, DiO, *etc*. These dyes were incorporated into EV membranes in a non-covalent way (mainly via hydrophobic interactions). To test the labeling stability, the labelled EVs were incubated with physiologically-related samples such as serum. After 12 h incubation, the DiI-labeled vesicles had a greater degree of fluorescence reduction, while their supernatants obtained by centrifugation had a certain degree of fluorescence enhancement (Supplementary **Figure S13**). This observation was attributed to the weak interactions between DiI dyes and phospholipids. The DiI dyes were prone to leach from the EV membranes, especially in the process of centrifugation, causing the decline of DiI fluorescence in EVs. We assumed that the free DiI dyes could assemble into micelle structures or/and adsorb onto lipoproteins in the supernatants to result in an increase of fluorescence. However, the Cy5 fluorescence of the covalently-labeled EVs maintained stable within the same incubation period and under the same centrifugation conditions. The high stability of this chemoenzymatic labeling method should make it quite useful for EVs tracking in cellular interactions.

EVs act as cell-to-cell communicators participating in many physiological processes. However, the internalization processes and uptake mechanisms of EVs toward recipient cells have not been clearly revealed yet. In this study, we used RAW264.7 cells, an immunophagocytic cell line that is preferentially recruited by breast cancer cells[37,38], to exploit the dynamic process and mechanisms of EVs uptake. To investigate this, we incubated RAW264.7 cells with Cy5-labeled EVs at 4 °C for 10 min for attachment, followed by tracking the uptake process of individual EVs towards live cells at 37 °C. We found that binding of EVs to filopodia induced a rapid lateral movement toward the cell body. Most EVs initially attached to the filopodia of live cells, and then moved along the filopodia to interact with plasma membrane.[39,40] It was also reported that filopodia could drive EVs for the uptake of cells[41], which could confirm that our labelling strategy is reliable. The snapshots and the whole trajectory of a particle (**Figure 4a**) showed that the EV was surfing along the cell surface, blocked by the plasma membrane, and then internalized into the cytosol (**Figure 4b**, see **Movie S1** in Supporting Information). The velocity vs time plot clearly demonstrated the three-stage internalization process of Cy5-EVs (**Figure 4c**). Furthermore, we analyzed the movements of Cy5-EVs in each stage, according to the relationship between mean square displacement (MSD) and time lag (**Figure 4d**).

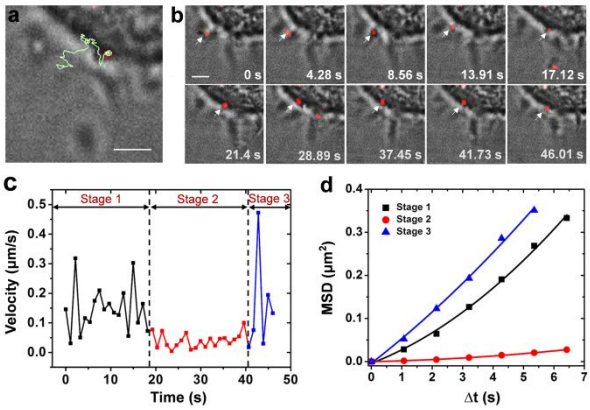


**Figure 4.** Real-time tracking of EV internalization processes by a RAW264.7 cell. (a) The whole trajectories of the Cy5-EV moving along filopodia. Scale bar: 2 μm. (b) The snapshots of the EV movements. Scale bar: 1 μm. (c) The instantaneous velocity *vs* time plot of EV shown in (a). (d) Mean square displacement (MSD) *vs* time lag (Δt) plot was calculated by using the points of the trajectory in each stage. The lines are the fit to MSD=4DΔt +(VΔt)$^2$+constant with D = 0.0068, 0.0004, 0.0137 μm$^2$/s and V = 0.064, 0.021, 0.0489 μm/s (D and V are the diffusion coefficient and fitting velocity, and the constant term is due to noise).

The movements of these three types were analyzed statistically with another three trajectories. According to the fits to MSD=4DΔt +(VΔt)$^2$+constant (D and V are the diffusion coefficient and velocity of the particle), the D and V values were calculated to be 0.0048 ±0.0016 μm$^2$/s and 0.0475 ±0.0121 μm/s(Mean ± Standard Deviation) at stage 1, 0.0003 ±0.0002 μm$^2$/s and 0.0140 ±0.0077 μm/s at stage 2, and 0.0117±0.0017 μm$^2$/s and 0.0469±0.0149 μm/s at stage 3, respectively ( Supplementary **Figure S14**). The apparent upward curves suggested that the movements could be characterized as directed motion along actin filaments. The diffusion coefficient and fitting velocity were consistent with the values of myosin motor protein-based movements.[38,39]

We asked whether the tracking method described here could be used for long-term monitoring of EVs internalization by live cells. The Cy5-labeled EVs were incubated with the adhered RAW264.7 cells at 37 °C for varying time. The fluorescent images were recorded by a confocal fluorescent microscope. **Figure 5a** shows that the Cy5-labeled EVs were gradually internalized by the RAW264.7 cells, as reflected by time-dependent fluorescence enhancement inside cells. The three-dimensional fluorescent image confirms the entry and distribution of the Cy5-labelled EVs (**Figure 5b**, Supplementary **Figure S15**). The time-dependent cellular entry of EVs was validated by flow cytometry (**Figure 5c**), which was commonly employed to quantify the fluorescent intensity of cell population. We noted that the EVs started to enter RAW264.7 cells at 1 h, and the fluorescence reached the maximum value at 8 h approximatively. We further employed the parental cells (MCF-7 cell) of EVs to evaluate the cell uptake process. Supplementary **Figure S16** shows that the Cy5-EVs can be internalized by MCF-7 cells and the uptake process was also time-dependent, which are similar with RAW264.7 cells. The findings were supported by flow cytometry analysis (Supplementary **Figure S17**). The uptake started at around 40 min and saturated at 8 h, wheras the intensity of internalization was weaker than that in RAW264.7 cells, mostly likely owing to the fact that RAW264.7 cells are macrophages that have a greater ability than normal cells to take up foreign substances.

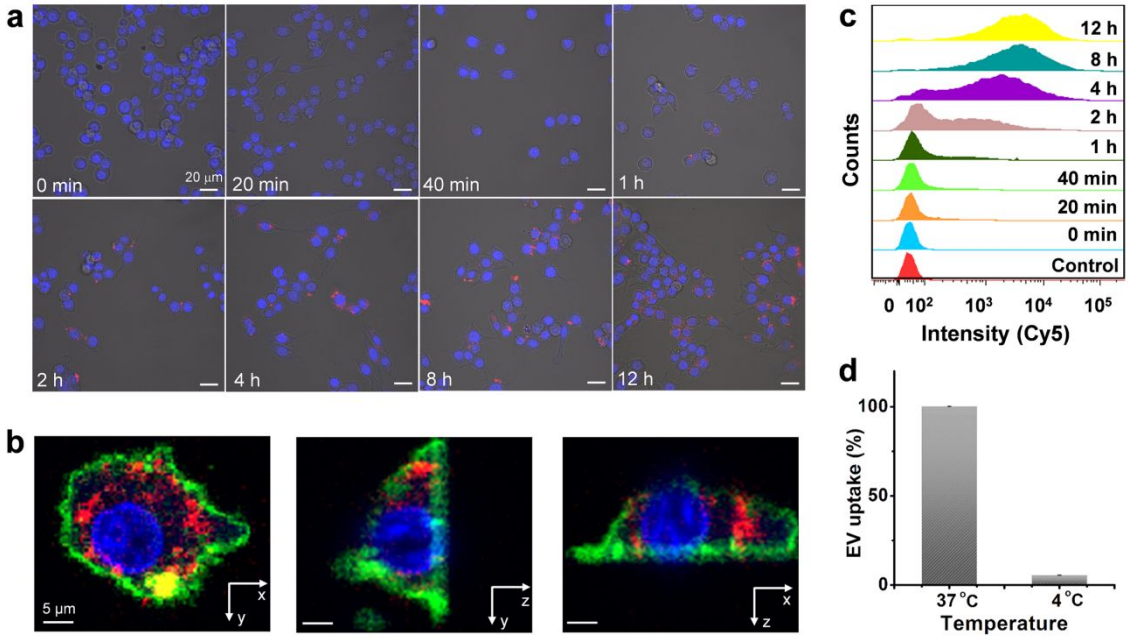


**Figure 5.** Long-term monitoring of EVs internalization by RAW264.7 cells. (a) Confocal fluorescence images of Cy5-EVs internalization by RAW264.7 cells at different time. The RAW264.7 cells were incubated with 20 μL Cy5-EVs (0.4 mg/mL). The cells were co-stained with Hoechst 33342. (b) Representative 3D images of a RAW264.7 cell that was treated with Cy5-EVs for 12 h. The first image shows xy slices, the second and last ones show orthogonal yz and xz views of the processed z stack respectively. Red, blue, and green indicate the Cy5-EVs, nucleus, and cell membrane respectively. (c) Flow cytometry analysis of EVs uptake at different time intervals. From bottom to up, the uptake time is increasing. (d) Flow cytometry quantitation analysis of cell internalization at normal temperature (37 °C) and low temperature (4 °C). In all samples, 10,000 cells were used. Data are shown as mean ± SD (n = 3).varying time. The fluorescent images were recorded by a confocal fluorescent microscope.

Furthermore, we observed that the intracellular fluorescence of ingested EVs at normal incubation temperature (37 °C) is 10-fold higher than that at low temperature (4 °C), indicating that the RAW264.7 cell uptake is a temperature-dependent process (**Figure 5d**). Notably, the EV uptake event is closely associated with energy consumption, which implies that the EV internalization by the macrophage cells relies on energy-dependent active endocytosis rather than energy-free membrane fusion. To confirm this, a set of RAW264.7 cells were treated with different concentrations of cytochalasin D (an actin polymerization inhibitor to suppress endocytic pathways)[42] before incubation with the Cy5-labeled EVs. The flow cytometry results showed that the treatment of cytochalasin D can reduce EV uptake in a dose dependent manner (Supplementary **Figure S18**).

The active cellular internalization of EVs depends on several endocytic pathways, including macropinocytosis, phagocytosis, clathrin-dependent endocytosis, and lipid raft-mediated endocytosis.[43] To explore the possible mechanisms, we used a set of representative inhibitors to block specific uptake pathways. 5-ethyl-N-isopropyl amiloride (EIPA), a macropinocytosis inhibitor that blocks $Na^+/H^+$ exchanger,[44] can largely inhibit the EVs uptake (**Figure 6a**). This result proves that macropinocytosis plays a crucial role in EV internalization by macrophages. Wortmannin, a typical phagocytosis inhibitor targeting phosphoinositide 3-kinase (PI3K),[45] can hinder membrane insertion into phagosomes. This result shows that phagocytosis can also impact the uptake of EVs (**Figure 6b**). The phagocytosis pathway emerges frequently in macrophages.[46] Interestingly, we found that EVs uptake was marginally reduced with the increased concentration of chlorpromazine (**Figure 6c**), a clathrin-mediated endocytosis (CME) inhibitor that interferes with the association between clathrin and the plasma membrane.[47] CME is a classical pathway for nanoparticle uptake particularly those with a size less than 120 nm.[48] In this study, however, the size distributions of EVs range roughly from 300 to 1000 nm (**Figure 3b**), causing few EVs can be uptaken via CME. Finally, we used methyl-β-cyclodextrin (MβCD)[49] to assess lipid raft-mediated endocytosis in the process of RAW264.7 uptake. However, MβCD did not influence EV uptake (**Figure 6d**). Collectively, the process of EVs internalization by RAW264.7 cells is mainly dependent on phagocytosis and macropinocytosis.

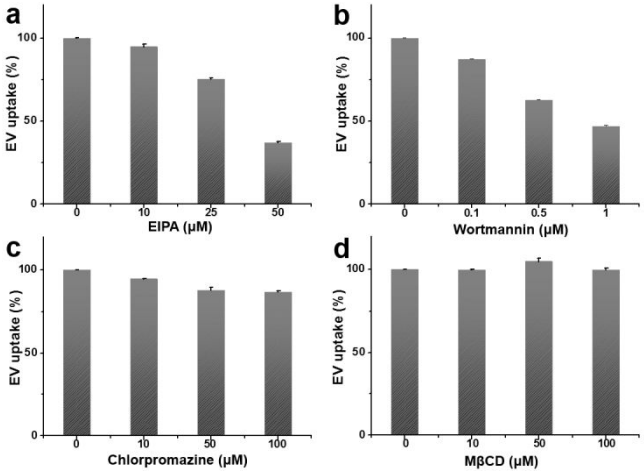


**Figure 6.** EV uptake by RAW264.7 cells after incubation with Cy5-EVs for 4 h in the presence of increasing concentrations of (a) EIPA, (b) wortmannin, (c) chlorpromazine, and (d) MβCD. The EV uptake was quantified by flow cytometry (BD LSR Fortessa) with excitation at a wavelength of 640 nm. The uptake of the control groups was defined to be 100% and other dosing groups were divided by the controls. Data are shown as mean ± SD (n = 3).

## CONCLUSIONS

In summary, a chemoenzymatic labeling strategy was for the first time constructed to directly engineer the native phosphatidylcholine of EVs with fluorescent dyes in situ. This labeling strategy is characteristic of high robustness and biocompatibility. As revealed by TEM and cell migration assays, the labeling strategy did not impact both morphology and biological activity of EVs, respectively. Moreover, unlike conventional dye-insertion methods, the chemoenzymatic labeling strategy enables the dye conjugation to EV phosphatidylcholine in a covalent fashion, endowing high chemical stability in diverse complex biological environments. Finally, the high performance of this labeling method was allowed to monitor the EV-cell interactions in real time, providing a powerful means to reveal the EV internalization mechanisms toward RAW264.7 cells. Overall, this study opens up a new platform for EV labeling, which should facilitate the investigation and application of EVs in biological and biomedical fields.

## ASSOCIATED CONTENT

**Supporting Information**

Supplementary figures and movie are included in the Supporting Information. This material is available free of charge via the internet at http://pubs.acs.org.

## AUTHOR INFORMATION

### Corresponding Author

*liudb@nankai.edu.cn.

**Notes**

The authors declare no competing financial interests.

## ACKNOWLEDGMENT

This study was supported by the National Natural Science Foundation of China (Grants 21775075 and 21977053), the Fundamental Research Funds for Central Universities (China), and the Thousand Youth Talents Plan of China.

## REFERENCES

(1) EL Andaloussi, S; Maeger, I; Breakefield, X O; Wood, M J A. *Nat. Rev. Drug Discov.* **2013,** *12,* 348-358.
(2) Shao, H L; Im, H; Castro, C M; Breakefield, X; Weissleder, R; Lee, H H. *Chem. Rev.* **2018,** *118,* 1917-1950.
(3) Mathieu, M; Martin-Jaular, L; Lavieu, G; Thery, C. *Nat. Cell Biol.* **2019,** *21,* 9-17.
(4) Colombo, M; Raposo, G; Thery, C. *Annu. Rev. Cell Dev. Bi.* **2014,** *30,* 255-289.
(5) Bronisz, A; Wang, Y; Nowicki, M O; Peruzzi, P; Ansari, K I; Ogawa, D; Balaj, L; De Rienzo, G; Mineo, M; Nakano, I; Ostrowski, M C; Hochberg, F; Weissleder, R; Lawler, S E; Chiocca, E A; Godlewski, J. *Cancer Res.* **2014,** *74,* 738-750.

(6) Hoshino, A; Costa-Silva, B; Shen, T L; Rodrigues, G; Hashimoto, A; Mark, M T; Molina, H; Kohsaka, S; Di Giannatale, A; Ceder, S; Singh, S; Williams, C; Soplop, N; Uryu, K; Pharmer, L; King, T; Bojmar, L; Davies, A E; Ararso, Y; Zhang, T; Zhang, H; Hernandez, J; Weiss, J M; Dumont-Cole, V D; Kramer, K; Wexler, L H; Narendran, A; Schwartz, G K; Healey, J H; Sandstrom, P; Labori, K J; Kure, E H; Grandgenett, P M; Hollingsworth, M A; de Sousa, M; Kaur, S; Jain, M; Mallya, K; Batra, S K; Jarnagin, W R; Brady, M S; Fodstad, O; Muller, V; Pantel, K; Minn, A J; Bissell, M J; Garcia, B A; Kang, Y; Rajasekhar, V K; Ghajar, C M; Matei, I; Peinado, H; Bromberg, J; Lyden, D. *Nature* **2015,** *527,* 329-335.

(7) Costa-Silva, B; Aiello, N M; Ocean, A J; Singh, S; Zhang, H Y; Thakur, B K; Becker, A; Hoshino, A; Mark, M T; Molina, H; Xiang, J; Zhang, T; Theilen, T M; Garcia-Santos, G; Williams, C; Ararso, Y; Huang, Y J; Rodrigues, G; Shen, T L; Labori, K J; Lothe, I M B; Kure, E H; Hernandez, J; Doussot, A; Ebbesen, S H; Grandgenett, P M; Hollingsworth, M A; Jain, M; Mallya, K; Batra, S K; Jarnagin, W R; Schwartz, R E; Matei, I; Peinado, H; Stanger, B Z; Bromberg, J; Lyden, D. *Nat. Cell Biol.* **2015,** *17,* 816-826.

(8) Buzas, E I; Gyorgy, B; Nagy, G; Falus, A; Gay, S. *Nat. Rev. Rheumatol.* **2014,** *10,* 356-364.

(9) Gyorgy, B; Hung, M E; Breakefield, X O; Leonard, J N. *Annu. Rev. Pharmacol.* **2015,** *55,* 439-464.

(10) Lyu, Y; Cui, D; Huang, J; Fan, W; Miao, Y; Pu, K. *Angew. Chem., Int. Ed.* **2019,** *58,* 4983-4987.

(11) Jiang, Y; Shi, M L; Liu, Y; Wan, S; Cui, C; Zhang, L Q; Tan, W H. *Angew. Chem., Int. Ed.* **2017,** *56,* 11916-11920.

(12) Wan, S; Zhang, L Q; Wang, S; Liu, Y; Wu, C C; Cui, C; Sun, H; Shi, M L; Jiang, Y; Li, L; Qiu, L P; Tan, W H. *J. Am. Chem. Soc.* **2017,** *139,* 5289-5292.

(13) Shen, W; Guo, K Z; Adkins, G B; Jiang, Q S; Liu, Y; Sedano, S; Duan, Y K; Yan, W; Wang, S E; Bergersen, K; Worth, D; Wilson, E H; Zhong, W W. *Angew. Chem., Int. Ed.* **2018,** *57,* 15675-15680.

(14) Zhao, Z; Yang, Y; Zeng, Y; He, M. *Lab Chip* **2016,** *16,* 489-496.

(15) Zhang, P; Zhou, X; He, M; Shang, Y Q; Tetlow, A L; Godwin, A K; Zeng, Y. *Nat. Biomed. Eng.* **2019,** *3,* 438-451.

(16) Armstrong, J P K; Holme, M N; Stevens, M M. *ACS Nano* **2017,** *11,* 69-83.

(17) Suetsugu, A; Honma, K; Saji, S; Moriwaki, H; Ochiya, T; Hoffman, R M. *Adv. Drug Deliver. Rev.* **2013,** *65,* 383-390.

(18) Lai, C P; Kim, E Y; Badr, C E; Weissleder, R; Mempel, T R; Tannous, B A; Breakefield, X O. *Nat. Commun.* **2015,** *6,* 7029.

(19) Smyth, T; Petrova, K; Payton, N M; Persaud, I; Redzic, J S; Gruner, M W; Smith-Jones, P; Anchordoquy, T J. *Bioconjugate Chem.* **2014,** *25,* 1777-1784.

(20) Dominkus, P P; Stenovec, M; Sitar, S; Lasic, E; Zorec, R; Plemenitas, A; Zagar, E; Kreft, M; Lenassi, M. *Bba-Biomembranes* **2018,** *1860,* 1350-1361.

(21) Mineo, M; Garfield, S H; Taverna, S; Flugy, A; De Leo, G; Alessandro, R; Kohn, E C. *Angiogenesis* **2012,** *15,* 33-45.

(22) Meckes, D G; Shair, K H Y; Marquitz, A R; Kung, C P; Edwards, R H; Raab-Traub, N. *Proc. Natl. Acad. Sci. U.S.A.* **2010,** *107,* 20370-20375.

(23) Tian, T; Zhu, Y-L; Zhou, Y-Y; Liang, G-F; Wang, Y-Y; Hu, F-H; Xiao, Z-D. *J. Biol. Chem.* **2014,** *289,* 22258-22267.

(24) Li, P; Zhang, R; Sun, H T; Chen, L; Liu, F; Yao, C; Du, M X; Jiang, X D. *Stem Cells Dev.* **2013,** *22,* 340-344.

(25) Lassailly, F; Griessinger, E; Bonnet, D. *Blood* **2010,** *115,* 5347-5354.

(26) Wiklander, O P B; Nordin, J Z; O'Loughlin, A; Gustafsson, Y; Corso, G; Mager, I; Vader, P; Lee, Y; Sork, H; Seow, Y; Heldring, N; Alvarez-Erviti, L; Smith, C I E; Le Blanc, K; Macchiarini, P; Jungebluth, P; Wood, M J A; Andaloussi, S E *J. Extracell. Vesicles* **2015,** *4,* 26316-26316.

(27) Zhang, P J; Dong, B; Zeng, E Z; Wang, F C; Jiang, Y; Li, D Q; Liu, D B. *Anal. Chem.* **2018,** *90,* 11273-11279.

(28) Morishita, M; Takahashi, Y; Nishikawa, M; Sano, K; Kato, K; Yamashita, T; Imai, T; Saji, H; Takakura, Y. *J. Pharm. Sci.* **2015,** *104,* 705-713.

(29) Selvy, P E; Lavieri, R R; Lindsley, C W; Brown, H A. *Chem. Rev.* **2011,** *111,* 6064-6119.

(30) Bumpus, T W; Baskin, J M. *Angew. Chem., Int. Ed.* **2016,** *55,* 13155-13158.

(31) Bumpus, T W; Baskin, J M. *ACS Central Sci.* **2017,** *3,* 1070-1077.

(32) Bumpus, T W; Liang, F J; Baskin, J M. *Biochemistry-Us* **2018,** *57,* 226-230.

(33) Hong, S L; Chen, T; Zhu, Y T; Li, A; Huang, Y Y; Chen, X. *Angew. Chem., Int. Ed.* **2014,** *53,* 5827-5831.

(34) Jeppesen, D K; Fenix, A M; Franklin, J L; Higginbotham, J N; Zhang, Q; Zimmerman, L J; Liebler, D C; Ping, J; Liu, Q; Evans, R; Fissell, W H; Patton, J G; Rome, L H; Burnette, D T; Coffey, R J. *Cell* **2019,** *177,* 428-445.

(35) Wan, Y; Cheng, G; Liu, X; Hao, S J; Nisic, M; Zhu, C D; Xia, Y Q; Li, W Q; Wang, Z G; Zhang, W L; Rice, S J; Sebastian, A; Albert, I; Belani, C P; Zheng, S Y. *Nat. Biomed. Eng.* **2017,** *1,* 0058.

(36) Caponnetto, F; Manini, I; Skrap, M; Palmai-Pallag, T; Di Loreto, C; Beltrami, A P; Cesselli, D; Ferrari, E. *Nanomed-Nanotechnol.* **2017,** *13,* 1011-1020.

(37) Mantovani, A; Marchesi, F; Malesci, A; Laghi, L; Allavena, P. *Nat. Rev. Clin. Oncol.* **2017,** *14,* 399-416.

(38) Xiong, F; Ling, X; Chen, X; Chen, J; Tan, J X; Cao, W J; Ge, L; Ma, M L; Wu, J. *Nano Lett.*. **2019,** *19,* 3256-3266.

(39) Chang, K; Baginskil, J; Hassan, S F; Mini, M; Shukla, D; Twari, V. *Front. Microbiol.* **2016,** *7*.

(40) Wang, Z-G; Liu, S-L; Tian, Z-Q; Zhang, Z-L; Tang, H-W; Pang, D-W. *ACS Nano* **2012,** *6,* 10033-10041.

(41) Heusermann, W; Hean, J; Trojer, D; Steib, E; von Bueren, S; Graff-Meyer, A; Genoud, C; Martin, K; Pizzato, N; Voshol, J; Morrissey, D V; Andaloussi, S E L; Wood, M J; Meisner-Kober, N C. *J. Cell Biol.* **2016,** *213,* 173-184.

(42) Casella, J F; Flanagan, M D; Lin, S. *Nature* **1981,** *293,* 302-305.

(43) Mayor, S; Pagano, R E. *Nat. Rev. Mol. Cell Bio.* **2007,** *8,* 603-612.

(44) Fitzner, D; Schnaars, M; van Rossum, D; Krishnamoorthy, G; Dibaj, P; Bakhti, M; Regen, T; Hanisch, U K; Simons, M. *J. Cell Sci.* **2011,** *124,* 447-458.

(45) Stephens, L; Ellson, C; Hawkins, P. *Curr. Opin. Cell Biol.* **2002,** *14,* 203-213.

(46) Kerr, M C; Teasdale, R D. *Traffic* **2009,** *10,* 364-371.

(47) Escrevente, C; Keller, S; Altevogt, P; Costa, J. *BMC Cancer* **2011,** *11,* 108.

(48) Yameen, B; Choi, W I; Vilos, C; Swami, A; Shi, J J; Farokhzad, O C. *J. Control. Release* **2014,** *190,* 485-499.

(49) Mulcahy, L A; Pink, R C; Carter, D R F *J. Extracell. Vesicles* **2014,** *3,* 24641.

For TOC only

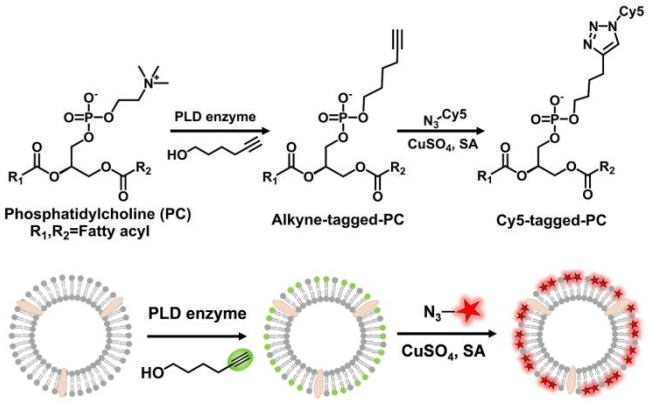
PLD enzyme
HO
$N_3$-Cy5
$CuSO_4$, SA
Cy5
Phosphatidylcholine (PC)
$R_1$,$R_2$=Fatty acyl
Alkyne-tagged-PC
Cy5-tagged-PC
PLD enzyme
HO
$N_3$
$CuSO_4$, SA